

2009

# Colloidal transport on magnetic garnet filmsw

Tierno Pietro
*Universitat de Barcelona*

Frances Sagues
*Universitat de Barcelona*

Tom H. Johansen
*University of Wollongong*, tomjo@uow.edu.au

Thomas Fischer
*Universita¨t Bayreuth*



## Publication Details

Tierno, P., Sagues, F., Johansen, T. H. and Fischer, T. (2009). Colloidal transport on magnetic garnet filmsw. Physical Chemistry Chemical Physics, 11 (42), 9615-9625.

# Colloidal transport on magnetic garnet films†

**Pietro Tierno,*[ab] Francesc Sagués,[ab] Tom H. Johansen[cd] and Thomas M. Fischer[e]**

***Received 27th May 2009, Accepted 31st July 2009***
***First published as an Advance Article on the web 25th August 2009***
**DOI: 10.1039/b910427e**

This article reports several recent discoveries related to the controlled transport of paramagnetic colloidal particles above magnetic garnet films. The garnet films are thin uniaxial ferromagnetic films in which ferromagnetic domains can be organized into symmetric patterns consisting of stripes or bubbles and generate strong local magnetic field gradients. Application of an external homogeneous magnetic field on a larger scale compared to the spatial periodicity of the magnetic pattern in the film modulates the potential generated at its surface and induces the controlled motion of colloidal particles placed above the film. Several novel dynamical regimes are observed and reported, from localized trajectories to direct particle transport, depending on the geometry of the underlying magnetic pattern and on the parameters, which control the external driving field, such as frequency, strength and direction. Moreover, we show that this strategy allows separation and sorting of bi-disperse particle systems based on the particle size as well as the transport of chemical or biological cargoes attached to the colloidal carriers. Controlled transport of micro-sized cargoes (chemical or biological) by colloidal particle carriers in a microfluidic environment can bring significant contributions in several fields from targeted drug delivery to the realization of precise fluid-based micro-scale devices.



## I. Introduction

Colloidal particles are very promising candidates for the controlled delivery of chemicals and drugs in fluid media on the small scale, since the particle surface can be chemically functionalized[1,2] and the available particle size ranges from tens of nms to hundreds of microns.[3,4] Another important advantage is that colloidal particles can be readily manipulated by applying relatively small forces, such as those obtained by optical,[5,6] electric,[7,8] magnetic[9,10] or thermal fields.[11,12] The last few years have witnessed many advances[13,14] in using light sources to manipulate and exert radiation pressure on micrometric colloidal particles.[15,16] Also precise trapping and manipulation over large ensembles of particles has been recently accomplished with the use of fast scanning light beams[17] and holographic optical techniques.[18] Electric fields are commonly used in electrophoresis[19,20] for the transport of colloidal particles subjected to a uniform

[a] *Departament de Química Física, Universitat de Barcelona, Martí i Franquès 1, Barcelona, 08028, Spain. E-mail: ptierno@ub.edu; Tel: +34-9340-20138*
[b] *Institut de Nanociència i Nanotecnologia, Universitat de Barcelona, Barcelona 08028, Spain*
[c] *Department of Physics, University of Oslo, Blindern, Norway*
[d] *Institute for Superconducting and Electronic Materials, University of Wollongong, NSW, Australia*
[e] *Institut für Experimentalphysik V, Universität Bayreuth, 95440 Bayreuth, Germany*

† Electronic supplementary information (ESI) available: Supplementary videos. See DOI: 10.1039/b910427e

**Pietro Tierno**

*Pietro Tierno studied physics at the University "Federico II" of Napoli. He received a PhD in Natural Sciences from the University of Ulm in 2005. After a postdoc at Florida State University, he moved to the University of Barcelona in 2007. His main research interests focus on soft matter systems with an emphasis on manipulation and transport of colloidal particles with external fields, propulsion in viscous fluids and microscale self-assembly phenomena.*

**Francesc Sagués**

*Francesc Sagués received his PhD at the University of Barcelona in 1983. After a postdoc at the University of Texas in Austin, he became associate professor and then full professor of physical chemistry in 2000 at the University of Barcelona. From his background in physical chemistry and statistical physics, his main research interests focus on self-organization processes of soft-matter and bio-inspired systems including monolayers, colloids, liquid crystals, biomembranes and biological tissues encompassing theoretical and experimental approaches.*

electric field and dielectrophoresis[21,22] when there is a field gradient. Controlled manipulation and trapping was also demonstrated in a microfluidic device exhibiting a topological ratchet-like structure by applying a low frequency electric field.[23]

A different way to transporting colloidal particles relies on the use of external magnetic fields, which is very attractive since such fields neither alter the fluid media nor affect biological cells. Magnetic particles can be moved in a fluid by using magnetic field gradients, *e.g.*, by holding a permanent magnet close to the colloidal suspension. This constitutes the principle of separation of magnetic particles from bulk suspensions on which many related techniques are based.[24–29] However, this method becomes inappropriate when precise control of the particle position and speed is required. Precise manipulation of individual microscopic particles requires magnetic fields that are heterogeneous on the particle scale. Various strategies have been adopted to create such field gradients. For example, Ramadan *et al.*[30–32] realized micro-coils on a Si substrate made by electroplated Cu trenches and with micron-size ferromagnetic pillars as magnetic cores. The magnetic field generated by this structure could guide and displace magnetic particles along the trenches. However, the coil configurations require alternate injection of current and could cause undesired local heating of the substrate. Alternatively, Mirowski *et al.*[33] used a cantilever tip in a microfluidic platform, as a "magneto-robotic" arm providing a movable local magnetic field gradient able to capture magnetic particles much like optical tweezers do. In principle, both methods allow precise control over the motion of one particle, but become unfeasible for large ensembles. A more convenient approach consists in using a magnetically structured substrate, *i.e.* a substrate with magnetic topographic patterns prepared on the particle scale. The periodic potential generated by these substrates can be modulated by applying an additional external homogeneous magnetic field and, depending on the pattern period relative to the particle size, transport of the latter could be obtained. Two notable examples in the literature are the works of Yellen *et al.*[34] and Gunnarson *et al.*[35] In both cases, magnetic patterned substrates were made by "top-down" techniques such as photolithography, metal evaporation and lift-off process. In ref. 34 the magnetic substrate consists of a rectangular array of cobalt micro-cylinders on a silicon substrate. Application of an external magnetic field rotating in a plane normal to the substrate allows transport of non-magnetic particles dispersed in a ferrofluid. In contrast, in ref. 35 the topographic reliefs in the substrate were magnetic elliptical islands made by permalloy and placed above a substrate in a staircase-like pattern. Applying an external magnetic field rotating now in the plane of the film modifies the stray field of the magnetic ellipses and creates a driving force for the motion of paramagnetic colloidal particles placed on the film.

Going beyond these achievements, we discuss here a new "bottom-up" approach for the controlled transport of paramagnetic colloidal particles which uses ferrite garnet films (FGFs). In these ferromagnetic films, when prepared with sufficiently strong uniaxial anisotropy, magnetic domains are formed and organize into lattices of stripes or bubbles having magnetization perpendicular to film. These domains, each one magnetized oppositely to the adjacent area, are easily modulated in size by applying magnetic fields with a perpendicular component. Thus, with a typical domain size of a few microns, the stray magnetic field on the FGF surface will have tunable modulations on the same scale. In the pioneering work by Goa *et al.* (and one of us),[36] the stray magnetic field generated from a mobile Bloch wall[37] (BW) inside an in-plane magnetized FGF, was used to manipulate vortices in a type-II superconductor. Afterwards, Helseth *et al.* (and some of us)[38,39] showed that the same principle of magnetic micro-manipulation could be applied to paramagnetic colloidal particles deposited above a FGF. Our strategy to transport paramagnetic colloidal particles consists in periodically modulating the magnetic landscape generated by the stray field of uniaxial FGFs.[40–42] When an aqueous solution of the particles is spread over the film, the particles are pinned to the BWs in the film due to the

**Tom H. Johansen**

*Tom H. Johansen is a full professor of physics at the University of Oslo. His main interests are: (i) the magnetic behaviour of superconductors, in particular avalanche dynamics in the vortex matter, and other non-linear phenomena studied experimentally with single flux quantum resolution using magneto-optical imaging (MOI), (ii) synthesis and characterization of single-crystal ferrite garnet films (FGFs) as high-sensitivity magnetic field sensors in MOI, and (iii) the use of FGFs as devices for pinning and manipulation of superconducting vortices and various kinds of magnetic microparticles, and also as reconfigurable chips for trapping of cold atoms.*

**Thomas M. Fischer**

*Thomas M. Fischer received his doctorate from the Johannes Gutenberg University in 1992 and held positions at University of California Los Angeles, the University of Leipzig, the Max Planck Institute of Colloids and Interfaces, and the Florida State University. Since 2007 he works at the University of Bayreuth. His research interests are on soft condensed matter dynamics at interfaces, where he focuses on the autonomous and driven motion of colloids and nano-systems.*

intense stray field generated at the surface. Application of an external magnetic field, which moves the BWs allows displacing and manipulating the colloidal particles. The key element in achieving direct controlled transport of paramagnetic colloids above a magnetic garnet is the conversion of a homogeneous time dependent external field into a spatially and temporally varying field on the FGF surface. The garnet film allows for adjustment of the typical length scale of the spatial heterogeneities down to the colloidal scale. Depending on the magnetic domain pattern (stripes or bubbles), the film thickness, and field parameters (strength, frequency or direction), one can achieve different modes of transport, from localized orbital motion to directed transport with particle speeds up to 200 μm $s^{-1}$. The main advantages in using FGFs with respect to lithography-made patterned substrates are (1) the possibility to externally control the pattern orientation before and during the particle motion; (2) the absence of topographic micro-reliefs, which can disturb the particle motion due to hydrodynamic or steric interactions. Moreover, the garnets are mechanically very robust materials, and inert to most chemicals, and thus can easily be integrated in microfluidic devices or used for other fluid based applications. Developing magnetically controlled transport of paramagnetic particles on surfaces adds a powerful new tool for biochemical and biophysical analysis to the arsenal of microscale technology.

In this perspective we describe recent results related to the controlled transport of paramagnetic colloidal particles placed above magnetic garnet films. We explore the variety of colloidal transport modes that can be triggered depending on the experimental conditions. We show that these transport modes lead to various applications for microfluidic devices such as digital colloidal shift registers, separation and sorting of colloidal bi-disperse systems and transport of chemical or biological cargoes. The paper is organized as follows: in section II we describe the magnetic garnet films and the response of these films to external magnetic fields. We also introduce the paramagnetic colloidal particles. Section III shows how to obtain particle motion above these films by applying external magnetic modulations. We show that depending on the magnetic pattern, different modes of transport are achievable, from digital particle motion (hopping) to continuous ballistic transport. FGFs can be used also as platforms to sort particles based on their size and this is described in section IV. The coupling of the particles with biological or chemical cargoes and their controlled transport above the magnetic film is described in section V. Section VI concludes this review by outlining promising future research directions.

## II. Uniaxial ferrite garnet films

### II.1 General requirement

The films creating the dynamic magnetic landscapes must be synthesized having in mind that a number of functional properties are critically important. In addition to (i) allow the formation of appropriate magnetic domain structures, the films must have (ii) a saturation magnetization, $M_s$, giving stray fields near the surface that create magnetic forces of proper magnitude on the particles, (iii) a strong Faraday effect to allow the domain walls and their motion to be visible using polarized light microscopy, and (iv) a very low coercivity so that the walls can move smoothly, *i.e.*, with a minimum of pinning and resulting intermittency. We have found that a class of materials where all these multi-functional properties come nicely together is the bismuth-substituted ferrite garnets, $(ReBi)_3(FeGa)_5O_{12}$, where Re is yttrium and one or more rare earth elements, grown as single crystalline films on gadolinium gallium garnet (GGG) substrates. In the present work we have used Re = Y, Lu and Pr.

### II.2 Film growth

To synthesize the FGFs we use the dipping liquid phase epitaxy method. Oxide powders of the constituent rare earths, bismuth, iron and gallium, as well as PbO and $B_2O_3$, are initially melted in a thick-walled platinum crucible. To ensure homogeneity of the solution a stirrer mixes the melt while being kept in the 3-zone resistive furnace at 1050 °C for 30 min. Prior to the film growth the melt temperature is reduced to around 700 °C, creating a supercooling of 50–70 K. The GGG substrate wafer is mounted horizontally in a 3-finger platinum holder attached to a shaft rotating by 60 rpm. After a period of pre-heating in the upper section of the furnace, the substrate is carefully lowered and locked in position once its lower side gets in contact with the melt. Subsequent growth from the supersaturated solution for 5–10 min results in a film of a few micron thickness. The substrate is then lifted slightly above the melt, and remaining droplets are removed by a rapid rotation. Finally, the film/substrate is cooled to room temperature sufficiently slow to minimize thermal stress. Before use, the film is cleaned in warm $HNO_3$ acid in an ultrasonic bath.

Successful growth also depends critically on the quality and type of substrate. We use 0.5 mm thick GGG wafers cut from Czochralski grown boules, up to 3 inch in diameter. They should have a minimum of striations and built-in stress, which is obtained by cutting the wafers perpendicular to the boule growth direction. The wafers are electrochemically polished providing an open surface for the epitaxial growth.

To make FGFs with magnetic domain patterns suitable for manipulation we use wafers cut from boules grown in the (111)-direction, resulting in a sufficiently large uniaxial anisotropy to make the spontaneous magnetization perpendicular to the film. Using wafers cut from (100)-grown boules can give in-plane magnetization films with a different domain structure which also allows magnetic manipulation, *e.g.*, of paramagnetic beads[43,44] and even superconducting vortices.[45–49] In this article we will review only the work done with the uniaxial FGFs.

### II.3 Films in a magnetic field

In a zero-applied field the uniaxial FGFs minimize their energy by forming magnetic domains. For manipulation purposes, the regular domain structures are of particular interest, and two types of periodic structures typically exist: (a) a 1D array of parallel stripes with alternating up/down

magnetization, and (b) a 2D lattice of cylindrical bubbles embedded inside a matrix of reverse magnetization.

When a magnetic field, $H_z$, is applied perpendicular to the film, the domains initially magnetized parallel to $H_z$ will increase in size at the expenses of the area of anti-parallel domains. This is illustrated in Fig. 1 (left), showing how a stripe domain structure evolves as the applied field increases from zero (top to bottom). This behaviour is well described by the model of Kooy and Enz,[50] who found a Fourier series solution to the problem of minimizing the total free energy, the latter consisting of the energy of magnetization in an applied field, the energy of the magnetic walls that separate the domains, and the demagnetization energy. Shown in Fig. 1 (right) are curves for the predicted domain widths as functions of the applied field. At small fields the width of the majority and minority domains, $\lambda_+$ and $\lambda_-$ change linearly with $H_z$, while the period of the stripe pattern, $\lambda = \lambda_+ + \lambda_-$, remains essentially constant. In this linear regime the overall domain pattern is quite robust, making the structure very well suited for applications. Note that this is not the case at higher fields where at some point both $\lambda_+$ and $\lambda$ diverge, accompanied by large deformations of the pattern itself, often starting with dislocation climbs (see lower image in Fig. 1).

The stripe period in a zero-applied field, $\lambda_0$, is determined by the ratio of the domain wall energy density and $\mu_0 M_s^2$, as well as the film thickness. Typical films used in the present work have $\lambda_0 \sim$ 2–15 μm. In the linear small field regime it follows from the Kooy and Enz model that the domain wall displacement, $x$, *vs.* applied field is given by:

$$x = \frac{\lambda_+ - \lambda_-}{2} = \frac{\pi t/2}{\ln\cosh(\pi t/\lambda_0)} \frac{H}{M_s},$$

where $t$ denotes the film thickness. For a FGF with $t$ = 4 μm, $\lambda_0$ = 10 μm, and $M_s$ = $10^4$ A m$^{-1}$, the wall displacement becomes $\Delta x$ = 1 μm for a $\Delta H_z$ = $10^3$ A m$^{-1}$ change in the applied field. Note that $2x/\lambda$ is the magnetization (normalized by $M_s$) of such stripe domain films, hence the above expression also gives the initial susceptibility.

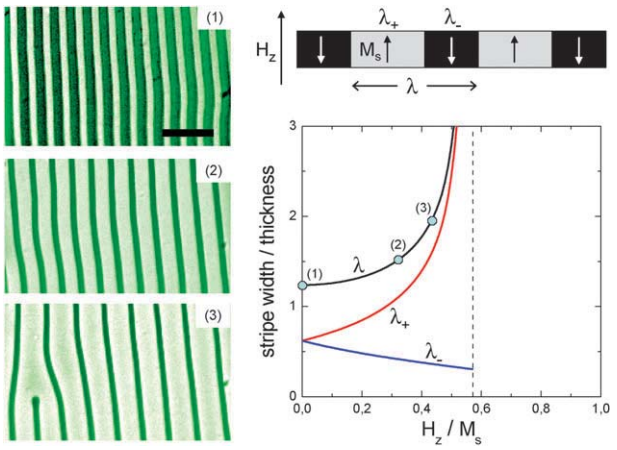


**Fig. 1** Left: magneto-optical images[79] of stripe domains in a uniaxial FGF (ferrite garnet film) in different magnetic fields, $H_z$, applied perpendicular to the film. The first image is for $H_z$ = 0, where the stripe period is $\lambda_0$ = 10 μm (scale bar 30 μm). Right (upper): side view of the domain configuration, (lower), the width of the majority and minority domains, $\lambda_+$ and $\lambda_-$, and their period $\lambda = \lambda_+ + \lambda_-$ *vs.* applied field normalized by the saturation magnetization, $M_s$ of the FGF. The positions on the $\lambda$ ($H_z$) curve marked (1)–(3) correspond to the images on the left.

A regular lattice of magnetic domains shaped as circular cylinders can be generated in the same type of FGFs by applying a series of high frequency (~10 kHz) magnetic field pulses of amplitude ~$3M_s$ and directed perpendicular to the film. The ac field breaks up the long stripe domains, and after this field is removed cylindrical bubbles magnetized axially, *i.e.*, normal to the film, self-organize into a hexagonal configuration embedded in a connected area of opposite magnetization. Similar to the stripe domain films, when subsequently applying a quasi-static field, the bubble domains will increase or decrease in diameter depending on the field being parallel or opposite to the bubble magnetization. For moderate applied fields the bubbles remain circular in shape and maintain the global lattice structure. More details about magnetic bubbles, and stripe domain behaviour, can be found in ref. 51.

### II.4 Paramagnetic colloidal particles

Paramagnetic colloidal particles[52] are micron-size polystyrene particles doped with small superparamagnetic iron oxide grains (size from 10 Å to few nms). These particles are commercially available as a monodisperse suspension in water. In the presence of relatively low magnetic fields $H$ ($<10^4$ A m$^{-1}$, particle magnetic saturation ~$10^5$ A m$^{-1}$ [53]), the particles become magnetized and acquire a dipole moment, which is proportional to the external field: $m = V\chi H$ where $\chi$ is the particle magnetic volume susceptibility and $V$ the particle volume. As a result the particles feel a force pointing in the direction of the gradient of the square of the magnetic field, $F \propto \nabla H^2$ and thus can be moved in a medium only in the presence of a gradient of the magnetic field. For these properties, paramagnetic particles are of great importance in both biological and physical sciences and they can be used to probe forces down to the fN range (1 fN = $10^{-15}$ N). For instance, these particles have been used to stretch[54] and manipulate[55] DNA, probe the cell environment,[56,57] assemble[58] and melt[59] colloidal crystals and study a variety of statistical phenomena.[60–63]

### II.5 Experimental details

In the experiments we used two kinds of paramagnetic particles from Dynal (Norway), with diameters $d_1$ = 1 μm and $d_2$ = 2.8 μm, and magnetic volume susceptibility $\chi_1$ = 1.1 and $\chi_2$ = 0.4 resp.[53,64] The particles, dispersed in water, are electrostatically stabilized by the negative charges acquired from the dissociation of the surface carboxylic groups (COO–). We diluted the original aqueous suspension of the particles with high deionized water (18.2 MΩ cm, MilliQ system) up to a density ~$10^7$ beads mL$^{-1}$ and deposit a few drops on top of the garnet film. Due to gravity, after a few minutes, the particles sediment above the film and are attracted toward the BWs. In some cases we observe some particles that stick to the surface of the film due to the strong attraction of the BWs. To avoid this problem we coat the

 

garnet with a thin layer of polysodium-4-styrene sulfonate, which acquires a negative charge in water.

The external homogeneous magnetic field used to modify the magnetic pattern of the film and, in turn move the colloidal particles, was applied by using a set of three orthogonal coils mounted on the rotating stage of a conventional polarization microscope (Leica DMPL or Nikon E400). Field modulations were achieved by connecting two such coils with a waveform generator (TTi-TGA1244) feeding a current amplifier (IMG STA-800 or KEPCO BP). Static magnetic fields were obtained by connecting one such coil with a dc power supply (TTi-EL302Tv). Various CCD cameras having 30–120 fps temporal resolution mounted on the polarization microscopes were used to observe the particles and the film. To measure the particle position and speed we record .AVI videos by using commercial frame-grabbing software (STREAMPIX, NORPIX). These videos were then analyzed frame by frame by using custom-made programs written in MATLAB and using the image processing toolbox.

## III. Transport of particles on garnet films

### III.1 Stripe patterned film

Directed motion of colloidal particles above a stripe patterned garnet film can be achieved by applying an external oscillating magnetic field $H$, which is linearly polarized in the $(x, z)$ plane with an angular frequency $\Omega$, and inclination $\vartheta$ with respect to the film normal ($z$ axis); $H = \hat{H}$ (sin $\vartheta$ sin $\Omega t$, 0, cos $\vartheta$ sin $\Omega t$) where: $\hat{H} = \sqrt{H_x^2 + H_y^2 + H_z^2}$ is the amplitude of the field. Fig. 2(a) shows a polarization microscope image of paramagnetic particles above a garnet film with spatial periodicity $\lambda = 10.9$ μm, subjected to a magnetic field with inclination $\vartheta \sim 40^\circ$ and amplitude $\hat{H} = 0.6M_s$ where the saturation magnetization of this garnet film is $M_s = 1.7\times10^4$ A m$^{-1}$. Superimposed to the image we show the trajectory of one such particle after ~2.1 s, its path being always normal to the stripe pattern ($x$ direction in this case). In Fig. 2(b), the corresponding $(x, y)$ positions are plotted *vs.* time. It follows that the motion consists of discrete steps in which particles jump along one domain every half cycle of the external magnetic field. The induced motion is completely reversible since inverting the sign of the applied field along the $x$ or $z$ direction reverses the particle motion. In Fig. 2(c) and 2(d) we illustrate the mechanism of motion. The $z$ component of the external field is normal to the film and displaces the domain walls by increasing (resp. decreasing) the width of the domains having parallel (resp. opposite) magnetization direction. The $x$ component alternates the pinning sites located at the BWs between strong and weak walls depending whether the magnetic field lines are parallel (antiparallel) to the field direction. This modulation occurs every half cycle and particles cross one domain due to the local gradient generated between adjacent BWs. If the external field would be normal to the surface $\vartheta = 0$, the hopping across the domains would occur periodically in the forward or backward direction. A finite external field inclination $\vartheta > 0$ ,is necessary to induce the particle motion. During the application of the field, each domain wall returns to its initial position after one cycle $T = 2\pi/\Omega$ while, particles advance by

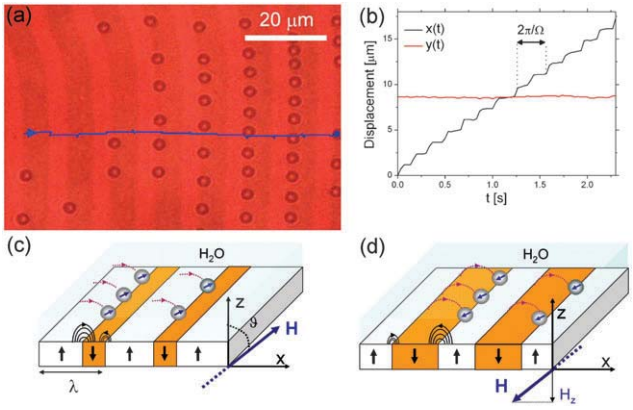


**Fig. 2** (a) Microscope image of paramagnetic colloidal particles transported above a stripe garnet film. One particle is marked in blue and the corresponding trajectory (blue line) is superimposed to the image. (b) Displacement *vs.* time of the colloidal particle shown in (a). The black [red] line refers to the $x(t)$ [$y(t)$] position. Part (c) and (d) illustrate the mechanism of motion in two half cycles of the external magnetic field. The particles hop by half the film spatial periodicity, $\lambda/2$ of the stripe pattern when reversing the magnetic field and changing strong domain walls into week domain walls. The movie (video 1) in the ESI† shows the particle transport above the magnetic stripe pattern.

one spatial periodicity of the stripe pattern. The particles pin to the domain walls when the external field is small $\Omega\tau \sim \pi/2 + n\pi$, $n = 0,1,2,3$, *etc.* and hop to the next domain wall during the times of maximum intensity of the external field $\Omega\tau \sim n\pi$, $n = 0,1,2,3$, *etc.* For the range of frequencies used ($0 < \Omega < 300$ s$^{-1}$), the domain walls follow instantaneously the external field and thus do not introduce any delay in the particle motion. We note that the mechanism of motion works well also for many particles since the colloids when initially deposited above the stripe form parallel chains. The external field induces dipolar interactions between the moving particles which are repulsive and keep the particle dispersed along the chain during motion. Dipolar interactions in the direction normal to the stripes are negligible due to the large separation of the domain walls with respect to the particle diameter. Thus the particle motion becomes essentially free of dispersion and allows to move the particles without losing information about their relative arrangement.

### III.2 Magnetic bubble array

Another way to achieve direct motion on an externally modulated garnet film is to use a magnetic bubble lattice. The two dimensional nature of the magnetic bubble array allows to extend the particles motion to the plane $(x, y)$ and more precisely, along the six crystallographic axes of the lattice. Let us consider one such particle located above the BW of a magnetic bubble that has circular symmetry. The film has a lattice constant $a = 10.7$ μm and the radius of the bubbles $R = 4.1$ μm. The external modulation is a precessing magnetic field composed of a rotating component in the $(x, y)$ plane plus a constant component along the $z$ direction; $H = \hat{H}$ (sin $\vartheta$ sin $\Omega t$, sin $\vartheta$ cos $\Omega t$, cos $\vartheta$) with $H_z = \hat{H}$ cos $\vartheta$. If $H_z = 0$, the particle rotates around the bubble with the frequency of the field. Fig. 3(a) shows the trajectories of the colloidal

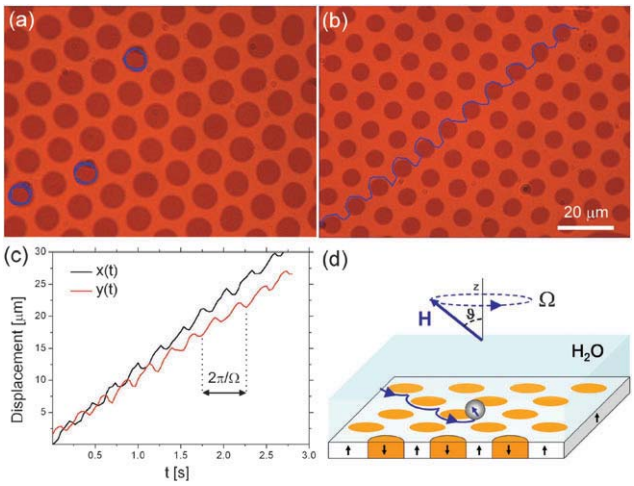


**Fig. 3** (a) Microscope image of paramagnetic particles rotating above a magnetic bubble film when subjected to a rotating magnetic field. (b) Motion of a paramagnetic colloidal particle subjected to a precessing magnetic field. The particle trajectories (blue line) are superimposed to the images. (c) Displacement *vs.* time of the colloidal particle shown in (b). Black [red] line refers to the $x(t)$ [$y(t)$] position. (c) Scheme showing a magnetic bubble lattice with a paramagnetic particle and subjected to a magnetic field $H$ precessing with frequency $\Omega$ and angle $\vartheta$ around the $z$ axis. The corresponding movies (videos 2 and 3) of Fig. 3(a) and (b) are deposited as ESI.†

particles subjected to an external magnetic field rotating with angular frequency $\Omega = 22.0\ s^{-1}$ and intensity $\hat{H} = 0.1\ M_s$ (precession angle $\vartheta = 90°$). The modulation modifies the magnetic stray field of the magnetic bubble and creates a gradient along the circular diameter which attracts the particle to some point in the circle. Rotating the field makes the minimum energy position rotates along the bubble edge and in turn drives the pinned colloidal particle. Such rotary particle motion could be used for example as a microscopic stirrer in order to mix fluids on a very small scale.[65] Application of the field $H_z$ reduces the size of the bubbles, enlarges the interstitial region between them, while the energy minima between adjacent bubble domains approach each other.[66] Below a certain value of $\vartheta$, or equivalently for sufficiently high value of $H_z$, the particles are able to cross between neighbouring domains instead of keeping circulating around them. This results in a net particle motion above the magnetic array as illustrated in Fig. 3(b) where the field precession angle is $\vartheta \sim 70°$. From the position ($x$, $y$) of the particle *vs.* time shown in Fig. 3(c) the 2D nature of the particle motion appears clearly.

Here we compare the mechanisms of particle motion in a stripe *vs.* bubble patterns. The main difference lies in the symmetry of the pattern, which allows 1D motion for parallel stripes (always normal to the stripes direction) and 2D motion for the magnetic bubble array. Also, the external modulation is different as it produces a motion composed of discrete steps for the stripe pattern, while it can be considered as a continuous driving in the second scenario. For both cases one can predict a linear behaviour of the particles velocity with the external driving expressed by $v = \Omega l/2\pi$ where $l$ is the characteristic length of the pattern which is equal to the spatial periodicity $\lambda$ (resp. lattice constant $a$) for the magnetic stripe (resp. bubble)

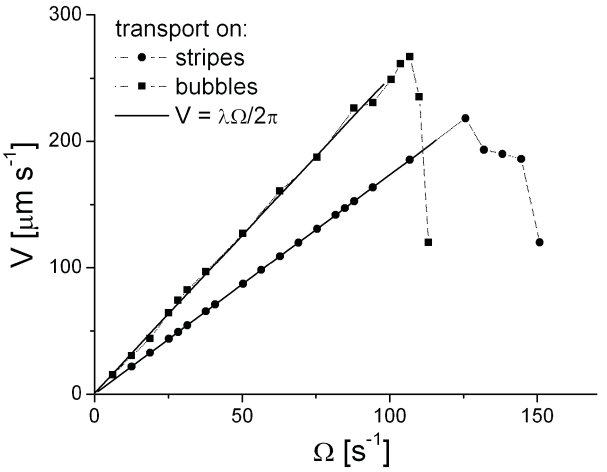


**Fig. 4** Velocity $v$ *vs.* external field frequency $\Omega$ for a paramagnetic colloidal particle above magnetic stripes (circles) and magnetic bubbles (squares) domains. Continuous lines are linear fits following the model $v = \lambda\Omega/2\pi$.

pattern. Fig. 4 shows $v$ *vs.* $\Omega$ for one paramagnetic colloidal particle above magnetic stripes (circles) and magnetic bubbles (squares) domains, where continuous lines are linear fits. The larger lattice constant as compared to the stripe spatial periodicity allows to reach higher speeds for the magnetic bubble lattice up to a maximum of 260 μm $s^{-1}$ for $\Omega = 100\ s^{-1}$. If the frequency is higher than a critical value, $\Omega > \Omega_c$, the viscous friction with the medium impedes the particles to follow the BW motion, and the velocity drops until the particles stop moving. We note that for the stripe pattern $\Omega_c = 125\ s^{-1}$ while we found a lower value for the hexagonal one $\Omega_c = 100\ s^{-1}$.

## IV. Particle separation and sorting

The trapping force by which a BW pins a paramagnetic particle depends mainly on the particle elevation above the surface of the film. Thus, smaller particles are more difficult to be released from the BWs than larger ones. The magnetic stray field diverges near the BWs and thus smaller particles experience a stronger field. We show here that this feature can be used to separate and sort colloidal particles based on their size by applying an external field too weak to move the smaller particles but strong enough for the large particles.

### IV.1 Sorting on striped patterned film

In Fig. 5 we show two microscope images (time separation 1.3 s) of a garnet film with a stripe pattern and having two populations of paramagnetic colloidal particles characterized by two diameters, $d_1 = 1$ μm (small particle) and $d_2 = 2.8$ μm (large particle). The trajectories of both particles, the small in green and the large in blue, are superimposed to the image. The external magnetic field has the form: $H = \hat{H}$ (sin $3\Omega t$, 0, sin $\Omega t$), with the in-plane component ($H_x$) oscillating with three times the frequency of the normal component ($H_z$). The motion of both particles occurs in discrete steps: during one half cycle of the field the small particle crosses the domain once (green trajectory in Fig. 5) while the large particle hops

 

three times that distance: twice in a upward and once in a downward direction (blue trajectory in Fig. 5). This is due to the particular form of the magnetic modulation and to a suitable choice of the field amplitude. Before reaching the maximum amplitude of forcing, the small particle stays fixed above the BW while the large particle, which is less attracted to the BW, has already hopped twice. When the field amplitude reaches its maximum value, the in-plane field changes its value and both particles are forced to hop almost synchronously. As a result both particles have moved in opposite directions and repeating the cycle several times results in a net particle separation. A more detailed explanation of the mechanism of separation can be found in ref. 41. Since particles are moving in opposite directions, accidentally one small and one large particle can collide. In this case the small particle slides over the surface of the larger one to follow the moving chain of small particles without affecting the separation mechanism. Also we note that this technique may be further refined to separate particles with three, four or five different sizes, for example by using more complex magnetic modulations having a planar component of the magnetic field with a frequency 5, 7 or 9 times the frequency of the normal field component.

### IV.2 Sorting on magnetic bubble arrays

The same principle of sorting based on particle size can be applied to a magnetic bubble lattice. This is illustrated in Fig. 6, which is composed of four microscope images showing two kinds of paramagnetic particles under an external precessing magnetic field. Again, superimposed to the images are the particle trajectories, in green for the small particle ($d_1$) and in blue for the large one ($d_2$). From Fig. 6(a) to Fig. 6(d) the normal component of the magnetic field $H_z$ was increased, *i.e.* the precession angle decreases, while the precession frequency was kept constant. The resulting particle dynamics can be summarized in the following modes: (a) both particles rotate around the magnetic bubbles, (b) the large particle moves above the magnetic lattice while the small particle continues the orbital motion, (c) both particles are transported and (d) the small particle is transported while the large remains localized. The particle sorting is achieved in (b) and (d) since

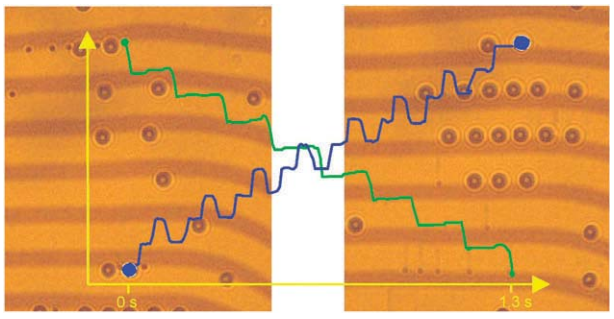


**Fig. 5** Polarization microscope images separated by a time interval of 1.3 s of a small (green) and large (blue) particles subjected to a Lissajou-like magnetic modulation (see text) having $\hat{H} = 8500$ A m$^{-1}$ and frequency $\Omega = 18.8$ s$^{-1}$. The tracked trajectories of the small (green) and large (blue) particles are superimposed to the images. The movie (video 4) in the ESI† shows the particle separation above the magnetic stripe pattern.

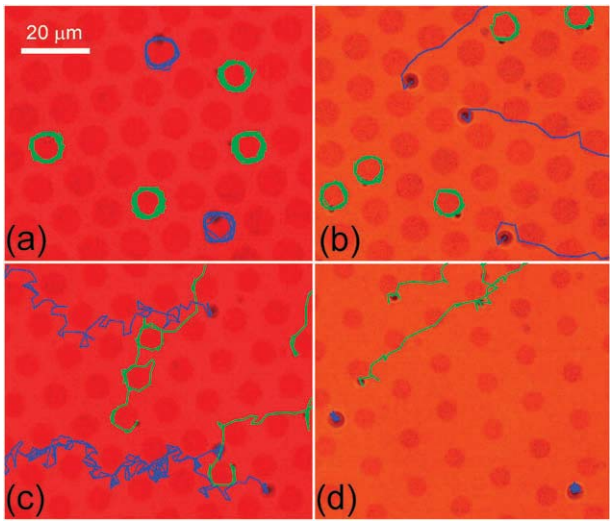


**Fig. 6** Polarization microscope images of a small and large particle above a garnet film and subjected to an external magnetic field with frequency $\Omega = 62.8$ s$^{-1}$ and components $\hat{H}_{xy} = 3100$ A m$^{-1}$ and $H_z = 0.12\ M_s$ (a), $H_z = 0.28\ M_s$ (b), $H_z = 0.41\ M_s$ (c) and $H_z = 0.56\ M_s$ (d). The garnet film used had saturation magnetization $M_s = 7.6 \times 10^3$ A m$^{-1}$. The tracked trajectories of the small (green) and large (blue) particles are superimposed to the images (image taken from ref. 80). The corresponding movies (videos 5a, 5b, 5c and 5d) of Fig. 6(a) to (d) are deposited as ESI.†

one type of colloid is localized around one magnetic bubble while the other is transported through the array and leaves the observation area. The difference between this sorting with respect to the previous one lies on the nature of the pattern. At high precession angles both particles circulate around the magnetic bubbles since the energy minima between adjacent bubbles are too separated for both particles. Increasing $H_z$ decreases $\vartheta$ and the size of the bubble making the energy minima closer. The large particle, which is less pinned to the BW is thus able to escape while the small particle continues to be localized. Still smaller precession angles are required to release both particles. We note that situation (d), where the small particle escapes and the large is localized, occurs because at the elevation of the large particle the energy minima are much closer than at the elevation of the small particle. The localization is in form of small triangular orbits which will equally occur at very low precession angle for the transport modes described in section III.2.

## V. Transport of cargoes on the microscale

One application of the motion of paramagnetic colloidal particles above magnetic garnet films is to load them with micro size cargos that can be delivered at certain locations above the film. All the following results will be demonstrated with garnet films having magnetic stripe domains, although they can be easily extended to the magnetic bubble array.

### V.1 Chemical cargoes

The simplest chemical cargo that can be transported in this way is an emulsion droplet attached by capillary forces to the colloidal particle. For example, Fig. 7(a) shows a spherical

droplet of silicon oil attached to a paramagnetic particle and transported above a stripe patterned film. The tracked particle (droplet) trajectory is superimposed to the three images in green (blue). Since the surface tension force dominates over the viscous force (capillary number Ca $\sim 10^{-6}$), the droplet is stable once attached to the colloidal particle and can be transported all over the film surface. The only way the cargo could be released would occur if the colloidal carrier enters a region with a second liquid in which the oil is miscible. This opens up various possibilities on the controlled delivery of very tiny amount of chemicals, which are encapsulated within the oil droplet. There is a limitation on the weight of the cargo that the paramagnetic particle can transport, which is dictated by the magnetic force exerted by the particle during each jump above the BW. This force which can be derived as $F = \mu_w \chi V \nabla(H_{tot} \cdot H_{tot})$ depends mainly on the particle size ($V$), its magnetic properties ($\chi$) and on the garnet film since $H_{tot} = H + H_{garnet}$ where $H_{garnet}$ is a function of the film spatial periodicity. Here $\mu_w$ is the magnetic susceptibility of the medium (water) in which the particle moves. Larger (resp. smaller) particles combined with a garnet film having smaller (resp. larger) stripe periods allow an increase (resp. decrease) of the amount of fluid transported. However, too large oil droplets can deposit and stick to the garnet surface, thus restraining this transport mechanism to emulsion droplets smaller than 8.5 μm in diameter. On the other hand there is no limitation over the smallness of the chemical cargoes which can go below the attolitre volume.

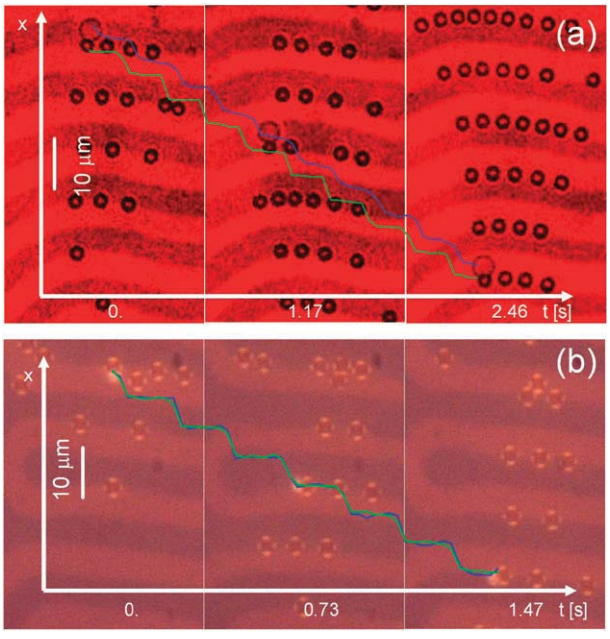


**Fig. 7** (a) Image sequence showing paramagnetic colloidal particles above a stripe pattern garnet film at three different times. Superimposed in green (blue) is the $x$ position *vs.* time (s) of one colloid (oil droplet). Corresponding movie (video 6) is deposited as ESI.† (b) Image sequence illustrating the transport of a small nematic droplet (blue trajectory) attached to one colloidal particle (green trajectory). In (b) the images were taken in reflected light mode. Corresponding movie (video 7) is deposited as ESI.†

A related example of transport of a chemical cargo is shown in Fig. 7b, where a small droplet of nematic liquid crystals (ZLI 1132) is attached to a paramagnetic colloidal particle and transported above a stripe pattern film. The microscopic images were taken in reflected light mode with crossed polarizers in order to observe the brightness of the LC droplet. In this observation mode the colloidal particles appear as round holes with four bright sides.[67] During application of the field, both the particle and the droplet follow the same trajectory with the green and blue paths almost superimposed. We notice that while the colloidal carrier shows the same brightness during all the recording time, the small nematic cargo changes periodically its luminosity, switching periodically from luminescent (state on) to dark (state off). This change in the droplet optical properties is shown in Fig. 8 composed of two polarization microscope images of a colloidal particle with an attached LC droplet before and during the hopping above the BW. It is well known that the orientation of the director in nematic liquid crystals, and thus the associated change in light intensity under crossed polarizers depends on several factors such as application of a magnetic field, fluid flow[68] or even changes in the boundary conditions of a droplet of LC. Competition between the surface alignment forces and the applied torque due to the external field, should govern the switching behaviour of the nematic droplet. In our particular case, the smallness of the droplet itself precludes in principle any kind of anchoring effect. We are thus left with the fluid flow and magnetic field as sources of this intriguing behaviour. One of these effects could be the reason for the observed change brightness. However the phenomenon requires more experimental analysis to be fully understood, but show the potentiality of our transport technique applied on chemical cargoes. For example it could be useful in applications related to opto-magnetic dimmer,[69] microscopic lighting system[70] or for magnetically controlled photonic applications.[71]

### V.2 Biological cargoes

Another useful application of the colloidal shift register based on magnetic garnet films relies on the transport of biological cells. It is possible to transport biological entities either by directly attaching the cell to the colloidal particle, as previously reported, or employing in a less invasive way, by using the secondary flow generated by an array of paramagnetic particles moving above the magnetic film. In Fig. 9(a) we show this principle as applied to yeast cells (*Saccharomyces cerevisiae*)

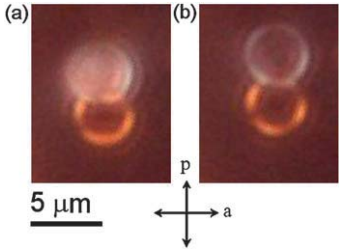


**Fig. 8** Polarization microscope images of a colloidal particle with an attached nematic LC droplet observed in reflected light enlarged to show the "on–off" effect (see text) before (a on) and during (b off) hopping of the particle along a BW.

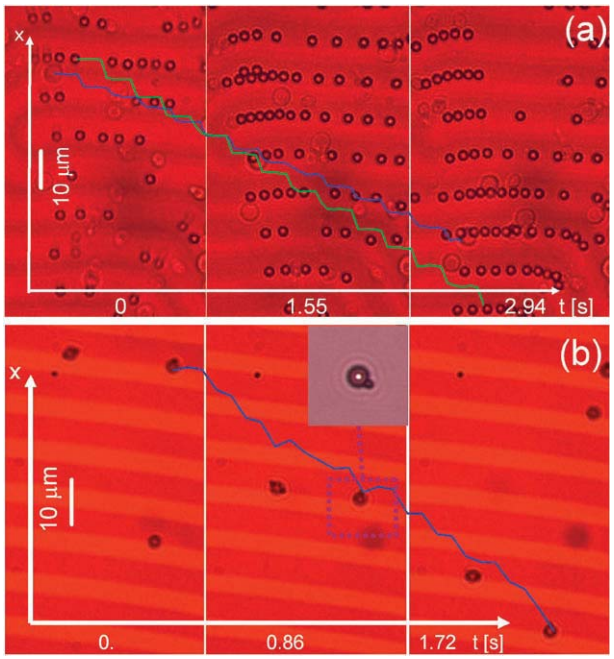


**Fig. 9** (a) Image sequence showing paramagnetic colloidal particles transporting yeast cells by secondary flow. The superimposed green (blue) trajectory indicates the $x$ position of one colloid (cell). The corresponding movie (video 8) is deposited as ESI.† (b) Polarization microscope images illustrating the motion ($x$ position in blue) of a composite particle made by linking two particles with different size through DNA bridge. The corresponding movie (video 9) is deposited as ESI.† The small microscope image on the top shows the asymmetric DNA-linked assembly (one small one large particle) on a glass plate.

dispersed in a water solution poured above a stripe pattern garnet film and containing a high density of paramagnetic colloidal particles. The three composed polarization microscopy images in Fig. 9(a) show the position of the paramagnetic particles and the yeast cells at different times while superimposed in green (resp. blue) is the trajectory of one colloidal particle (resp. yeast cell). Once deposited above the film the cells floated slightly higher than the particles due to their lower density ($\sim$1.1 g cm$^{-3}$) and the fact that the latter are attracted by the domain walls. Application of the external magnetic modulation set the particles in motion and generates a flow field, which drags the cells in the same direction. In contrast to the previous mechanism of motion, where each cargo was attached to one individual particle, here many more particles compared to the number of cells are needed to generate sufficient secondary flow. In these conditions the cells are moving with roughly one-half the speed of the particles. However, this technique allows to displace biological cells on a surface without use of external pressure gradients, which are necessary in conventional microfluidics devices.[72,73]

As stated in the introduction, one advantage of using paramagnetic colloidal particles is that their surface can be chemically functionalized in order to attach DNA molecules and this in turn offers the possibility to use biotin labelled DNA as a linker to form composite colloidal particles.[74,75] To show the potentiality of this method, and demonstrate the transport of DNA molecules, we realized an asymmetric doublet by attaching complementary biotin labelled single strands of DNA onto streptavidin-coated paramagnetic particles with different size (1.0 μm and 2.8 μm in diameter). Watson–Crick base pairing between the complementary 25 base pairs DNA-strands provided a link between the different sized particles that remained stable at room temperature. Fig. 9b shows the trajectory of one such doublet (blue line) above a garnet film where in the upper inset of the second microscopy image an individual doublet above a glass plate is shown. The same high speeds as for the individual particles (up to 200 μm s$^{-1}$) are achievable. Moreover several assemblies, larger than the elementary doublet are possible by using the DNA linking procedure (detailed described in ref. 76 and 77) and be transported by combining different particles with the same or different size.

Last we also mention the possibility to use our magnetic colloidal propulsion technique to transport specific biological cells such as microphages, by direct ingestion of paramagnetic particles.[78] In this special way, macrophages phagocytize paramagnetic particles or ferrofluids and can be transported across the garnet film after ingestion of the carrier.

## VI. Conclusions

Developing magnetic techniques that enable the controlled transport of colloidal particles in fluid media or microfluidic devices could find applications in several field related to the controlled delivery of drugs on the small scale. Due to the small size of the magnetic carriers, these techniques should rely on magnetic fields that vary on the length scale of the particles. Magnetic domains in FGFs could be used as a source of such spatially heterogeneous magnetic fields. Moreover, the domain structures of these films change when applying external magnetic fields. We have shown how to use these garnet films to convert external time dependent magnetic fields applied on a cm scale into magnetic fields heterogeneous on the micron scale in order to manipulate paramagnetic colloidal particles immersed in a fluid above the garnet film. This opens new the possibilities to investigate a large variety of colloidal transport phenomena: from localized orbits to directed motion and sorting capabilities; transport phenomena that can be fully controlled by specific magnetic patterns of the garnet film and by proper external magnetic field modulation.

All experiments shown in the preceding sections involve colloidal particles in the micron size range above magnetic patterns which were easily imaged with conventional optical microscopy. However, the proposed mechanism can be in principle down-scaled to the nanoscale. Patterns on the garnet film are usually of the order of the film thickness. It is thus possible to grow garnet films with patterns of smaller spatial periodicity, although their visualization would become challenging. If we refrain from visualizing the domains we might still follow the motion of quantum dots or single molecules attached to the carriers by using fluorescence techniques. The trapping strength at the domain walls depends on the width of the domains and the thickness of the film. We expect that, if we miniaturize the film, the trapping strength would decrease. This however, would be compensated by the decrease in size of the paramagnetic carriers used. Smaller

carriers can be closer to the domain wall and hence trapped stronger than larger carriers. As a consequence we expect the magnetic transport to be still effective upon miniaturization. These arguments hold as long as the paramagnetic particles are large compared to the domain wall width. When the particles are of the same size as the width of the magnetic domains, the magnetic transport becomes less effective and thermal fluctuations like Brownian motion may play a crucial role.

## Acknowledgements

P. T. was supported by "Beatriu de Pinós" program contract no. BP-B100167. F. S. and P. T. acknowledges financial support by MEC (project no. FIS2006-03525) and DURSI (contract no. 2005SGR00653). T. M. F. acknowledges support from the German Science Foundation (DFG) *via* the research unit FOR608. T. H. J. is grateful to The Research Councils of Norway and Australia for financial support.



## References

1 R. Pashley and M. Karaman, in *Applied Colloid and Surface Chemistry*, ed. John Wiley and Son, 2004.
2 R. J. Hunter, in *Foundations of Colloid Science*, ed. Clarendon Press, Oxford, 1989.
3 W. B. Russel, D. A. Saville and W. R. Schowalter, *Colloidal Dispersions*, Cambridge University Press, Cambridge, 1995.
4 *Colloidal Polymers (Surfactant Science)*, ed. A. Elaissari, Marcel Dekker, New York, 2003.
5 A. Chowdhury, B. J. Ackerson and N. A. Clark, *Phys. Rev. Lett.*, 1985, **55**, 833.
6 M. P. MacDonald, G. C. Splading and K. Dholakia, *Nature*, 2003, **426**, 421.
7 R. C. Hayward, D. A. Saville and I. A. Aksay, *Nature*, 2000, **404**, 56.
8 A. Yethiraj and A. van Blaaderen, *Nature*, 2003, **421**, 513.
9 G. Helgesen, P. Pieranski and A. T. Skjeltorp, *Phys. Rev. Lett.*, 1990, **64**, 1425.
10 S. Melle, O. G. Calderón, M. A. Rubio and G. G. Fuller, *Phys. Rev. E: Stat., Nonlinear, Soft Matter Phys.*, 2003, **68**, 041503.
11 Z. D. Cheng, W. B. Russell and P. M. Chaikin, *Nature*, 1999, **401**, 893.
12 R. Piazza, *J. Phys.: Condens. Matter*, 2004, **16**, S4195.
13 D. G. Grier, *Nature*, 2003, **424**, 810–816.
14 K. C. Neuman and S. M. Blocka, *Rev. Sci. Instrum.*, 2004, **75**, 2787–2809.
15 A. Ashkin, J. M. Dziedzic, J. E. Bjorkholm and S. Chu, *Opt. Lett.*, 1986, **11**, 288–290.
16 S. M. Block, *Nature*, 1992, **360**, 493–5.
17 C. Mio, T. Gong, A. Terray and D. W. M. Marr, *Rev. Sci. Instrum.*, 2000, **71**, 2196.
18 E. R. Dufresne and D. G. Grier, *Rev. Sci. Instrum.*, 1998, **69**, 1974.
19 M. Medebach and T. Palberg, *Colloids Surf., A*, 2003, **222**, 175.
20 D. Mizuno, Y. Kimura and R. Hayakawa, *Langmuir*, 2000, **16**, 9547.
21 H. A. Pohl, *Dielectrophoresis*, Cambridge University Press, Cambridge, 1978.
22 T. B. Jones, *Electromechanics of Particles*, Cambridge University Press, Cambridge, 1995.
23 C. Marquet, A. Buguin, L. Talini and P. Silberzan, *Phys. Rev. Lett.*, 2002, **88**, 168301.
24 M. Takayasu, R. Gerber and F. J. Friedlaender, *IEEE Trans. Magn.*, 1983, **19**, 2112–2114.
25 R. Gerber, M. Takayasu and F. J. Friedlaender, *IEEE Trans. Magn.*, 1983, **19**, 2115–2117.
26 C. Cowen, F. J. Friedlaender and R. Jaluria, *IEEE Trans. Magn.*, 1976, **12**, 466–470; C. Cowen, F. J. Friedlaender and R. Jaluria, *IEEE Trans. Magn.*, 1976, **12**, 898–900.
27 T. M. Vickrey and J. A. Garciaramirez, *Sep. Sci. Technol.*, 1980, **15**, 1297–1304.
28 J. Y. Hwang, M. Takayasu, F. J. Friedlaender and G. Kullerud, *J. Appl. Phys.*, 1984, **55**, 2592–2594.
29 N. Pamme, *Lab Chip*, 2006, **6**, 24.
30 Q. Ramadana, Y. Chen, V. Samper and D. P. Poenar, *Appl. Phys. Lett.*, 2006, **88**, 032501.
31 Q. Ramadan, V. D. Samper, D. P. Puiu and C. Yu, *J. Microelectromech. Syst.*, 2006, **15**, 624.
32 Q. Ramadana, V. Samperb, D. Poenara and C. Yu, *J. Magn. Magn. Mater.*, 2004, **281**, 150–172.
33 E. Mirowski, J. Moreland, A. Zhang, S. E. Russek and M. J. Donahue, *Appl. Phys. Lett.*, 2005, **86**, 243901.
34 B. B. Yellen, O. Hovorka and G. Friedman, *Proc. Natl. Acad. Sci. U. S. A.*, 2005, **102**, 8860–8864.
35 K. Gunnarsson, P. E. Roy, S. Felton, J. Pihl, P. Svedlindh, S. Berner, H. Lidbaum and S. Oscarsson, *Adv. Mater.*, 2005, **17**, 1730.
36 P. E. Goa, H. Hauglin, Å. A. F. Olsen, D. Shantsev and T. H. Johansen, *Appl. Phys. Lett.*, 2003, **82**, 79–81.
37 The transition layer separating two domains with opposite magnetization directions.
38 L. E. Helseth, T. M. Fischer and T. H. Johansen, *Phys. Rev. E: Stat., Nonlinear, Soft Matter Phys.*, 2003, **67**, 042401.
39 L. E. Helseth, H. Z. Wen, T. M. Fischer and T. H. Johansen, *Phys. Rev. E: Stat., Nonlinear, Soft Matter Phys.*, 2003, **68**, 011402.
40 P. Tierno, S. V. Reddy, T. H. Johansen and T. M. Fischer, *Phys. Rev. E: Stat., Nonlinear, Soft Matter Phys.*, 2007, **75**, 041404.
41 P. Tierno, S. V. Reddy, J. Yuan, T. H. Johansen and T. M. Fischer, *J. Phys. Chem. B*, 2007, **111**, 13479.
42 P. Tierno, S. V. Reddy, M. G. Roper, T. H. Johansen and T. M. Fischer, *J. Phys. Chem. B*, 2008, **112**, 3833.
43 L. E. Helseth and T. M. Fischer, *Langmuir*, 2004, **20**, 8192.
44 L. E. Helseth, T. H. Johansen and T. M. Fischer, *Phys. Rev. E: Stat., Nonlinear, Soft Matter Phys.*, 2005, **71**, 062402.
45 P. E. Goa, H. Hauglin, A. A. F. Olsen, D. Shantsev and T. H. Johansen, *Appl. Phys. Lett.*, 2003, **82**, 79.
46 J. I. Vestgården, D. V. Shantsev, T. H. Johansen, Y. M. Galperin, P. E. Goa and V. V. Yurchenko, *Phys. Rev. Lett.*, 2007, **98**, 117002.
47 L. E. Helseth, T. M. Fischer and T. H. Johansen, *Phys. Rev. Lett.*, 2003, **91**, 208302.
48 L. E. Helseth, H. Z. Wen, R. W. Hansen, T. H. Johansen, P. Heinig and T. M. Fischer, *Langmuir*, 2004, **20**, 7323.
49 L. E. Helseth, T. M. Fischer, R. W. Hansen and T. H. Johansen, *Appl. Phys. Lett.*, 2004, **85**, 2556.
50 C. Kooy and V. Enz, *Philips Res. Reports*, 1960, **15**, 76.
51 A. H. Eschenfelder, *"Magnetic Bubble Technology". Springer Series in Solid State Sciences*, Springer-Verlag, Berlin, vol. 14, 1981.
52 These particles are usually referred as "super" paramagnetic due to their strong magnetization under external field compared to paramagnetic materials.
53 L. E. Helseth, *J. Phys. D: Appl. Phys.*, 2007, **40**, 3030.
54 S. B. Smith, L. Finzi and C. Bustamante, *Science*, 1992, **258**, 1122.
55 P. S. Doyle, J. Bibette, A. Bancaud and J. L. Viovy, *Science*, 2002, **295**, 2237.
56 C. Gosse and V. Croquette, *Biophys. J.*, 2002, **82**, 3314.
57 X. Trepat, L. Deng, S. S. An, D. Navajas, D. J. Tschumperlin, W. T. Gerthoffer, J. P. Butler and J. J. Fredberg, *Nature*, 2007, **447**, 592–595.
58 P. Tierno, T. M. Fischer, T. H. Johansen and F. Sagués, *Phys. Rev. Lett.*, 2008, **100**, 148304.
59 K. Zahn, R. Lenke and G. Maret, *Phys. Rev. Lett.*, 1999, **82**, 2721.
60 K. Zahn, J. M. Mendez and G. Maret, *Phys. Rev. Lett.*, 1997, **79**, 175.
61 Q.-H. Wei, C. Bechinger and P. Leiderer, *Science*, 2000, **287**, 625.
62 N. Osterman, D. Babič, I. Poberaj, J. Dobnikar and P. Ziherl, *Phys. Rev. Lett.*, 2007, **99**, 248301.
63 P. Tierno and W. A. Goedel, *J. Chem. Phys.*, 2005, **122**, 094712.
64 L. Clime, B. L. Drogoff and T. Veres, *IEEE Trans. Magn.*, 2007, **43**, 2929.
65 P. Tierno, T. H. Johansen and T. M. Fischer, *J. Phys. Chem. B*, 2007, **111**, 3077.
66 A. Soba, P. Tierno, T. M. Fischer and F. Sagués, *Phys. Rev. E: Stat., Nonlinear, Soft Matter Phys.*, 2008, **77**, 060401.

 

67 L. Helseth and T. M. Fischer, *Opt. Express*, 2004, **12**, 3428–3435.
68 A. F.- Nieves, D. R. Link, M. Márquez and D. A. Weitz, *Phys. Rev. Lett.*, 2007, **98**, 087801.
69 L. E. Helseth, H. Z. Wen and T. M. Fischer, *Langmuir*, 2006, **22**, 3941–3944.
70 F. E. Osterloh, *J. Am. Chem. Soc.*, 2002, **124**, 6248–6249.
71 X. Xu, S. A. Majetich and S. A. Asher, *J. Am. Chem. Soc.*, 2002, **124**, 13864–13868.
72 T. M. Squires and s. R. Quake, *Rev. Mod. Phys.*, 2005, **77**, 977–1026.
73 G. M. Whitesides, *Nature*, 2006, **442**, 368.
74 M. P. Valignat, O. Theodoly, J. C. Crocker, W. B. Russel and P. M. Chaikin, *Proc. Natl. Acad. Sci. U. S. A.*, 2005, **102**, 4225.
75 V. T. Milam, A. L. Hiddessen, J. C. Crocker, D. J. Graves and D. A. Hammer, *Langmuir*, 2003, **19**, 10317.
76 P. Tierno, R. Golestanian, I. Pagonabarraga and F. Sagués, *J. Phys. Chem. B*, 2008, **112**, 16525–16528.
77 P. Tierno, S. Schreiber, W. Zimmermann and T. M. Fischer, *J. Am. Chem. Soc.*, 2009, **131**, 5366–5367.
78 P. Dhar, P. Tierno, J. Hare, T. H. Johansen and T. M. Fischer, *J. Phys. Chem. B*, 2007, **111**, 13097.
79 P. E. Goa, H. Hauglin, M. Baziljevich, E. Il'yashenko, P. L. Gammel and T. H Johansen, *Supercond. Sci. Technol.*, 2001, **14**, 729.
80 P. Tierno, A. Soba, T. H. Johansen and F. Sagués, *Appl. Phys. Lett.*, 2008, **93**, 214102.